Analysis of Guided Waves in Inhomogeneous Bianisotropic Cylindrical Waveguides

Bernhard Jakoby, *Member, IEEE*, and Daniël De Zutter, *Member, IEEE*

Abstract— **Electromagnetic fields in structures composed of inhomogeneous cylindrical layers are analyzed using a propagator matrix approach. The presented formulation is capable of analyzing fully bianisotropic media, where the involved propagator matrix for bianisotropic media is derived in cylindrical coordinates. The applicability of the method is demonstrated by calculating the dispersion characteristics of surface waves as well as fundamental and higher order modes on cylindrical microstrip lines on top of an inhomogeneous bianisotropic substrate.**

I. Introduction

DUE TO ADVANCES in material science, analysis methods for electromagnetic waves in complex media have gained increasing interest. The most general linear medium is the so-called bianisotropic medium, which is described by four material tensors [1]. Several known analytical and numerical methods for ordinary isotropic media have been generalized in order to include more complex media as well. Apart from the coverage of general bianisotropic media, this paper focuses on cylindrical structures featuring lateral (angular) inhomogeneities. Cylindrically stratified structures are frequently used for waveguiding structures and may also be employed to model curved structures in an approximate way (see [2] for a general review).

Spectral domain analysis methods have proved to be powerful tools for the analysis of planar stratified media problems in electromagnetism for more than two decades now. Apart from the treatment of stratified isotropic media geometries, the approach is capable of handling structures consisting of fully bianisotropic media [3].

Cylindrically layered structures involving isotropic media have been analyzed in various configurations. For instance, quasistatic approaches have been employed utilizing spectral iterative techniques for multiconductor transmission lines [4] and conformal mapping procedures for elliptical configurations [5]. A problem featuring a special kind of inhomogeneity in angular direction introduced by a perfectly conducting wedge has been treated by means of a separation Ansatz [6]. Full wave solutions have been reported for microstrip patch antennas on cylindrical, homogeneous, and isotropic substrates [7]. The cited works represent typical approaches and contain further references to earlier works.

Manuscript received April 10, 1995; revised November 12, 1995. This work was supported by an Erwin Schrödinger Grant (J00975-TEC) from the Austrian Fonds zur Förderung der wissenschaftlichen Forschung.

The authors are with the Department of Information Technology, Electromagnetics Group, University of Gent, B-9000 Gent, Belgium.

D. De Zutter is also with the National Science Foundation of Belgium.

Publisher Item Identifier S 0018-9480(96)01452-4.

Recently, we dealt with a method-of-analysis for stratified planar structures involving bianisotropic layers being periodically inhomogeneous in the transverse direction [8]. These computations were based on the derivation of an eigenoperator equation which enabled the calculation of eigenmodes suitable for setting up expansions for the fields. The method presented in this paper can be interpreted as a generalization of the planar approach. However, in cylindrical coordinates it is not possible to eliminate the radial coordinate from the occurring eigenoperator matrix, which in general does not permit a simple calculation of eigenmodes as in the planar case. Hence we do not expand the fields in terms of eigenmodes, but calculate propagator matrices that give a relation between the transverse fields at the boundaries of inhomogeneous, bianisotropic, cylindrical layers. Finally we remark, that this approach principally also has been proposed by Chew for homogeneous isotropic and anisotropic media (in the latter case homogeneous material tensors in rectangular coordinates are considered) [2].

II. Theory

Assuming a time dependence $\exp(j\omega t)$, Maxwell's equations for inhomogeneous bianisotropic media read

$$\nabla \times \mathbf{H}(\mathbf{r}) = j\omega \underline{\underline{\xi}}(\mathbf{r}) \cdot \mathbf{E}(\mathbf{r}) + j\omega \underline{\underline{\xi}}(\mathbf{r}) \cdot \mathbf{H}(\mathbf{r}), \tag{1}$$

$$\nabla \times \mathbf{E}(\mathbf{r}) = -j\omega \underline{\underline{\mu}}(\mathbf{r}) \cdot \mathbf{H}(\mathbf{r}) - j\omega \underline{\underline{\zeta}}(\mathbf{r}) \cdot \mathbf{E}(\mathbf{r}) \tag{2}$$

where we used the EH (Tellegen) representation of the constitutive equations [1]. Adopting a cylindrical coordinate system (r, ϕ, z), the r components of the field vectors can be eliminated from the field equations in such a way that we can write

$$\underline{\underline{\mathcal{L}}} \cdot \mathbf{f} = \frac{\partial}{\partial r}\mathbf{f} \tag{3}$$

with

$$\mathbf{f} = \begin{bmatrix} f_1 \\ f_2 \\ f_3 \\ f_4 \end{bmatrix} = \begin{bmatrix} E_\phi \\ E_z \\ H_\phi \\ H_z \end{bmatrix} \tag{4}$$

and

$$\underline{\underline{\mathcal{L}}} = \underline{\underline{\mathcal{L}}}\left(r, \frac{\partial}{\partial \phi}, \frac{\partial}{\partial z}, \varepsilon_{kl}, \mu_{kl}, \xi_{kl}, \zeta_{kl}\right) \tag{5}$$

where $\varepsilon_{kl}, \mu_{kl}, \xi_{kl}$ and ζ_{kl} stand for the elements of the material parameter tensors in cylindrical coordinates $(k, l = r, \phi, z)$. Formally, the operator matrix $\underline{\underline{\mathcal{L}}}$ can be constructed

0018–9480/96$05.00 © 1996 IEEE

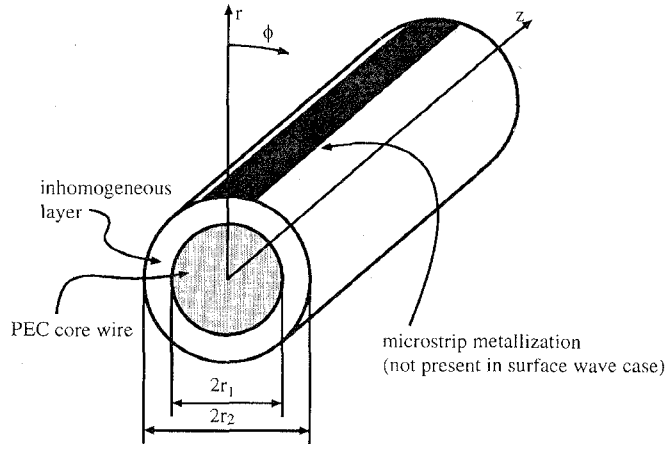

Fig. 1. Geometry of the problem.

from that of the planar case given in [8], [9] as shown in the Appendix.

This formulation is best suited for the analysis of cylindrically layered structures as shown in Fig. 1. The operator matrix can be cast into an algebraic matrix by transforming it to the spectral domain. As we want to deal with guided waves in the z-direction, we assume z-dependent fields according to $\exp(-jk_z z)$ (common factors $\exp(-jk_z z)$ will frequently be suppressed in the sequel). Noting further, that fields and material parameters must obey a 2π periodicity with respect to ϕ, we can expand these quantities as Fourier series

$$\psi(r,\phi,z) = e^{-jk_z z} \sum_{n=-\infty}^{\infty} \tilde{\psi}_n(r,k_z) e^{-jn\phi}, \tag{6}$$

$$g(r,\phi) = \sum_{n=-\infty}^{\infty} \tilde{g}_n(r) e^{-jn\phi} \tag{7}$$

where ψ represents any field component f_i $(i = 1 \cdots 4)$ and g denotes a function only depending upon material parameters. Note that we assumed the material parameters to be constant with respect to the direction of propagation z. The Fourier series coefficients $\tilde{g}_n(r)$ are given by

$$\tilde{g}_n(r) = \frac{1}{2\pi} \int_{-\pi}^{+\pi} g(r,\phi) e^{jn\phi} d\phi \tag{8}$$

and similarly for $\tilde{\psi}_n(r,k_z)$. Due to the fact, that the material parameters are independent of z, derivatives with respect to z can simply be replaced by $-jk_z$. In contrast, the expansions with respect to ϕ lead to an infinite-dimensional matrix equation in the expansion coefficients of the fields. This can be seen by considering the typical functions occuring in the evaluation of the expression $\underline{\underline{\mathcal{L}}} \cdot \mathbf{f}$

$$g\psi, \tag{9}$$

$$g\frac{1}{r}\frac{\partial}{\partial\phi}\psi, \tag{10}$$

$$\frac{1}{r}\frac{\partial}{\partial\phi} g\psi, \tag{11}$$

$$\frac{1}{r}\frac{\partial}{\partial\phi} g \frac{1}{r}\frac{\partial}{\partial\phi}\psi. \tag{12}$$

Substituting the expansions (6) and (7) into the above expressions, multiplying by $\exp(jm\phi)/2\pi$ and integrating over one period in ϕ leads to the mth Fourier series coefficients of the periodic expressions (9) to (12) with m going from $-\infty$ to $+\infty$

$$\sum_{n=-\infty}^{\infty} \tilde{g}_{m-n}\tilde{\psi}_n, \tag{13}$$

$$\frac{1}{r}\sum_{n=-\infty}^{\infty} \tilde{g}_{m-n}(-jn)\tilde{\psi}_n, \tag{14}$$

$$\frac{-jm}{r}\sum_{n=-\infty}^{\infty} \tilde{g}_{m-n}\tilde{\psi}_n, \tag{15}$$

$$\frac{-jm}{r^2}\sum_{n=-\infty}^{\infty} \tilde{g}_{m-n}(-jn)\tilde{\psi}_n. \tag{16}$$

These expressions represent convolutions of discrete spectra. Accordingly, in general each spectral field component is related to all other spectral components "mode conversion." Hence the operator (3) can formally be rewritten as an infinite dimensional matrix equation in terms of the spectral field components

$$\underline{\underline{\tilde{\mathbf{L}}}} \cdot \tilde{\mathbf{F}} = \frac{\partial}{\partial r}\tilde{\mathbf{F}} \tag{17}$$

where

$$\tilde{\mathbf{F}} = \begin{bmatrix} \vdots \\ \tilde{\mathbf{f}}_1 \\ \tilde{\mathbf{f}}_0 \\ \tilde{\mathbf{f}}_{-1} \\ \vdots \end{bmatrix}. \tag{18}$$

Here $\tilde{\mathbf{f}}_n$ denotes a vector containing the nth Fourier series coefficients of the vector function $\mathbf{f}$. The matrix $\underline{\underline{\tilde{\mathbf{L}}}}$ can be set up from $\underline{\underline{\mathcal{L}}}$ in a straightforward manner by using (13) to (16). For numerical treatment, this equation has to be truncated. The effects of the truncation will be discussed below. In the special case of laterally homogeneous media (i.e., with ϕ independent material parameters) the convolution series degenerate into a single term and the spectral field coefficients become decoupled.

Equation (17) represents a differential equation in the radial coordinate r. If the matrix $\underline{\underline{\tilde{\mathbf{L}}}}$ were independent of r, its solution could formally be written as

$$\tilde{\mathbf{F}} = \exp(\underline{\underline{\tilde{\mathbf{L}}}} r) \cdot \mathbf{c} \tag{19}$$

where $\mathbf{c}$ denotes a coefficient vector. This would represent a solution in terms of an infinite set of eigenmodes, each obeying a r-dependence $\exp(\lambda r)$, with λ being an eigenvalue of $\underline{\underline{\tilde{\mathbf{L}}}}$. In the planar case, the operator matrix is indeed independent of the normal coordinate (along the axis of stratification) and hence solutions corresponding to (19) can be used to expand the field in regions where the material parameters are constant with respect to the axis of stratification [8]. In the circular case, however, even for constant material parameters with respect to r, the matrix $\underline{\underline{\tilde{\mathbf{L}}}}$ depends on r due to several $1/r$ terms (see also the Appendix). In the special case of homogeneous isotropic

cylindrical structures, this leads to the well known eigenmodes in terms of Hankel functions rather than exponential functions [2]. In the general inhomogeneous and bianisotropic case, closed form eigensolutions cannot be derived, though.

For a given cylindrical layer with inner and outer radius r_1 and r_2, respectively, the differential (17) can be integrated in order to construct a propagator matrix $\underline{\underline{\mathbf{P}}}$ which relates the transversal field components at r_1 to those at r_2 in the following way

$$\tilde{\mathbf{F}}(r_2) = \underline{\underline{\mathbf{P}}}(r_2, r_1) \cdot \tilde{\mathbf{F}}(r_1). \tag{20}$$

Formally, the propagator matrix is given by

$$\underline{\underline{\mathbf{P}}}(r_2, r_1) = \exp \int_{r_1}^{r_2} \underline{\underline{\tilde{\mathbf{L}}}}(r) dr \tag{21}$$

where a possible r-dependence of the material parameters is considered as well. Numerically, the propagator matrix can be calculated by, e.g., subdividing the layer into L sublayers being so thin that $\underline{\underline{\tilde{\mathbf{L}}}}$ is assumed to be constant with respect to r within a sublayer

$$\underline{\underline{\mathbf{P}}}(r_2, r_1) \approx \prod_{n=L-1}^{0} (\underline{\underline{\mathbf{I}}} + \underline{\underline{\tilde{\mathbf{L}}}}(r_1 + n\Delta r)\Delta r). \tag{22}$$

Here $\underline{\underline{\mathbf{I}}}$ denotes the unit matrix and Δr is the thickness of a sublayer

$$\Delta r = \frac{r_2 - r_1}{L}. \tag{23}$$

In this paper we consider configurations as shown in Fig. 1 where an inhomogeneous cylindrical layer is covering a perfectly conducting wire with radius r_1. Hence all Fourier series coefficients related to tangential electric fields at r_1 must vanish

$$\tilde{E}_{\phi,n}(r_1) = \tilde{E}_{z,n}(r_1) = 0 \quad \text{or} \quad \tilde{f}_{1,n}(r_1) = \tilde{f}_{2,n}(r_1) = 0. \tag{24}$$

For the present, let us assume an impressed transverse current distribution at r_2. The fields expressed in (20) represent the fields just below the interface $r = r_2$ as the current distribution introduces jump discontinuities for the transverse field components. In the following, we denote the radial coordinate just below and above the interface $r = r_2$ by r_2^- and r_2^+, respectively.

Next we establish relations between the transverse fields at $r = r_2^+$. The ϕ-components in the homogeneous, isotropic region $r \geq r_2^+$ can be expressed in terms of the z-components

$$\begin{bmatrix} E_\phi \\ H_\phi \end{bmatrix} = \frac{1}{\omega^2\mu\varepsilon - k_z^2} \begin{bmatrix} \frac{1}{r}\frac{\partial}{\partial\phi}\frac{\partial}{\partial z} & j\omega\mu\frac{\partial}{\partial r} \\ -j\omega\varepsilon\frac{\partial}{\partial r} & \frac{1}{r}\frac{\partial}{\partial\phi}\frac{\partial}{\partial z} \end{bmatrix} \cdot \begin{bmatrix} E_z \\ H_z \end{bmatrix}. \tag{25}$$

The corresponding spectral fields are decoupled due to the homogeneity of the region; thus for a given ϕ-dependence $\exp(-jn\phi)$ we can substitute

$$\frac{\partial}{\partial\phi} \to -jn. \tag{26}$$

From the field solutions in source-free homogeneous, isotropic media, it is well known that E_z and H_z fulfill Bessel's differential equation. Hence they can be expressed as linear combinations of Hankel functions of first and second kind, $H_n^{(1)}(k_r r)$ and $H_n^{(2)}(k_r r)$, respectively. Here k_r denotes the radial wavenumber

$$k_r = \begin{cases} \sqrt{\omega^2\varepsilon\mu - k_z^2}; & \omega^2\varepsilon\mu > k_z^2, \\ -j\sqrt{k_z^2 - \omega^2\varepsilon\mu}; & \omega^2\varepsilon\mu < k_z^2 \end{cases} \tag{27}$$

where here and in the following we assume k_z to be real-valued. With this definition of k_r, the radiation condition at infinity requires that we consider Hankel functions of second kind only, which represent outward traveling or exponentially vanishing fields as $r \to \infty$. Setting

$$\tilde{E}_{z,n}(r) = AH_n^{(2)}(k_r r), \quad \tilde{H}_{z,n}(r) = BH_n^{(2)}(k_r r) \tag{28}$$

we can express the ϕ-components of the fields in terms of the coefficients A and B, or equivalently by the z-components at some given radius r_0 within the homogeneous region. Using (25) this leads to

$$\begin{bmatrix} \tilde{E}_{\phi,n}(r) \\ \tilde{H}_{\phi,n}(r) \end{bmatrix} = \underline{\underline{\mathbf{F}}}_n(r, r_0) \cdot \begin{bmatrix} \tilde{E}_{z,n}(r_0) \\ \tilde{H}_{z,n}(r_0) \end{bmatrix} \tag{29}$$

where

$$\begin{aligned} \underline{\underline{\mathbf{F}}}_n(r, r_0) &= \begin{bmatrix} F_{11,n} & F_{12,n} \\ F_{21,n} & F_{22,n} \end{bmatrix} \\ &= \frac{1}{\omega^2\mu\varepsilon - k_z^2} \\ &\quad \times \begin{bmatrix} -\frac{nk_z}{r}\frac{H_n^{(2)}(k_r r)}{H_n^{(2)}(k_r r_0)} & j\omega\mu k_r \frac{H_n^{(2)\prime}(k_r r)}{H_n^{(2)}(k_r r_0)} \\ -j\omega\varepsilon k_r \frac{H_n^{(2)\prime}(k_r r)}{H_n^{(2)}(k_r r_0)} & -\frac{nk_z}{r}\frac{H_n^{(2)}(k_r r)}{H_n^{(2)}(k_r r_0)} \end{bmatrix}. \end{aligned} \tag{30}$$

Here $H_n^{(2)\prime}$ denotes the derivative of $H_n^{(2)}$ with respect to its argument. Hence $\underline{\underline{\mathbf{F}}}_n(r_2, r_2)$ describes the relation between the transverse fields at $r = r_2^+$.

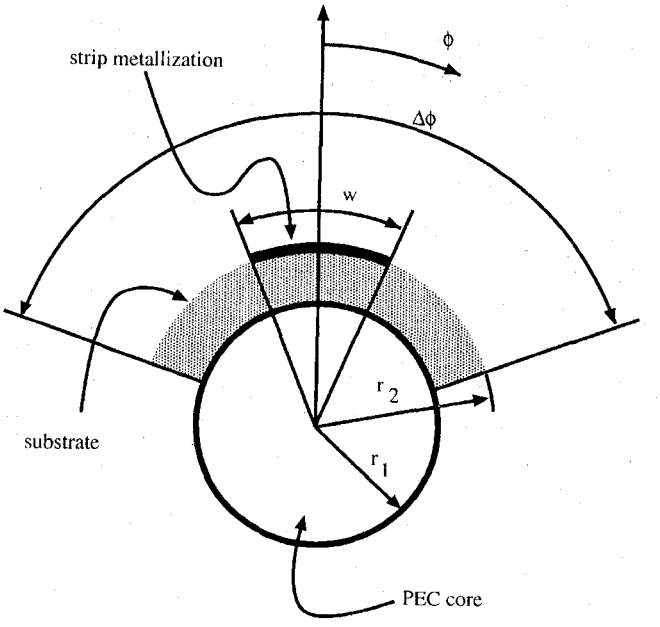

Fig. 2. Layer with angular inhomogeneity. The metallization is present only in the microstrip case.

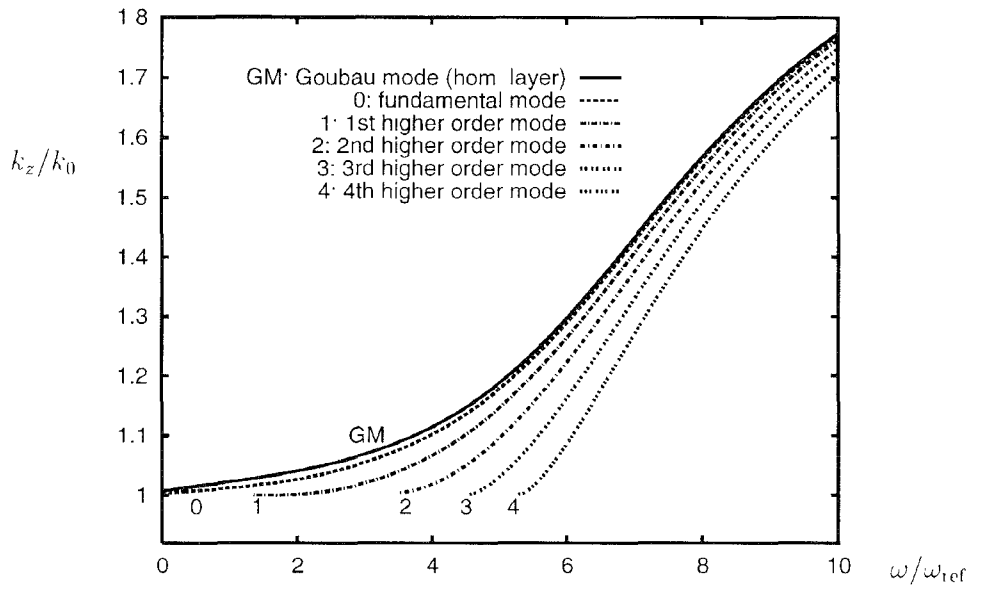

Fig. 3. Surface wave dispersion curves for a wire partially coated with an isotropic dielectric ($\varepsilon_r = 5$, $\Delta\phi = \pi$, $r_2/r_1 = 1.1$, $k_{\rm ref} r_1 = 1$) compared to that of the "Goubau mode" on the corresponding homogeneous layer ($\Delta\phi = 2\pi$)

To find the fields for a given transverse current distribution, we establish the following system of equations from the jump conditions at the interface r_2 and by considering conditions (24)

$$\begin{bmatrix} \underline{\underline{\mathbf{P}}}^{23} & \underline{\underline{\mathbf{P}}}^{24} & -\underline{\underline{\mathbf{I}}} & \underline{\underline{0}} \\ \underline{\underline{\mathbf{P}}}^{43} & \underline{\underline{\mathbf{P}}}^{44} & \underline{\underline{0}} & -\underline{\underline{\mathbf{I}}} \\ \underline{\underline{\mathbf{P}}}^{13} & \underline{\underline{\mathbf{P}}}^{14} & -\underline{\underline{\mathbf{F}}}^{11} & -\underline{\underline{\mathbf{F}}}^{12} \\ \underline{\underline{\mathbf{P}}}^{33} & \underline{\underline{\mathbf{P}}}^{34} & -\underline{\underline{\mathbf{F}}}^{21} & -\underline{\underline{\mathbf{F}}}^{22} \end{bmatrix} \cdot \begin{bmatrix} \vec{\tilde{f}}_3(r_1) \\ \vec{\tilde{f}}_4(r_1) \\ \vec{\tilde{f}}_2(r_2^+) \\ \vec{\tilde{f}}_4(r_2^+) \end{bmatrix} = \begin{bmatrix} -\vec{\tilde{M}}_\phi^S \\ \vec{\tilde{J}}_\phi^S \\ \vec{\tilde{M}}_z^S \\ -\vec{\tilde{J}}_z^S \end{bmatrix}. \tag{31}$$

Here we introduced the following symbols: vectors marked by arrows are set up by the spectral Fourier coefficients of a quantity, e.g.

$$\vec{\tilde{f}}_3(r_1) = \begin{bmatrix} \vdots \\ \tilde{f}_{3,1}(r_1) \\ \tilde{f}_{3,0}(r_1) \\ \tilde{f}_{3,-1}(r_1) \\ \vdots \end{bmatrix} = \begin{bmatrix} \vdots \\ \tilde{H}_{\phi,1}(r_1) \\ \tilde{H}_{\phi,0}(r_1) \\ \tilde{H}_{\phi,-1}(r_1) \\ \vdots \end{bmatrix}. \tag{32}$$

The vector $\vec{\tilde{f}}_i$ must not be confused with the vector $\tilde{\mathbf{f}}_l$ introduced earlier (see (18)). The latter represents a four-dimensional vector containing the lth Fourier coefficients of the vector $\mathbf{f}$, while the vector $\vec{\tilde{f}}_i$ is infinite-dimensional and is set up by all Fourier coefficients of the transverse field $f_i (i = 1 \cdots 4)$. In other words, the matrices $[\ldots, \tilde{\mathbf{f}}_1, \tilde{\mathbf{f}}_0, \tilde{\mathbf{f}}_{-1} \ldots]$ and $[\vec{\tilde{f}}_1, \vec{\tilde{f}}_2, \vec{\tilde{f}}_3, \vec{\tilde{f}}_4]$ are the transpose of each other. Accordingly, the matrices $\underline{\underline{\mathbf{P}}}^{kl}$ are composed of those elements of $\underline{\underline{\mathbf{P}}}(r_2, r_1)$ that relate $\vec{\tilde{f}}_k(r_2^-)$ and $\vec{\tilde{f}}_l(r_1)$. The matrices $\underline{\underline{\mathbf{F}}}^{lm}$ represent diagonal matrices being set up by matrix elements $F_{lm,n}$ given in (30); the matrix elements of $\underline{\underline{\mathbf{F}}}^{lm}$ read

$$F_{ij}^{lm} = \begin{cases} F_{lm,i}; & i = j, \\ 0; & i \neq j. \end{cases} \tag{33}$$

J_ν^S (M_ν^S) with $\nu = \phi, z$ denotes the electric (magnetic) surface currents residing in the interface r_2. The rows in (31) successively represent the jump conditions on the transverse fields E_z, H_z, E_ϕ, H_ϕ due to surface currents $M_\phi^S, J_\phi^S, M_z^S, J_z^S$, respectively. Hence, for a given interface current distribution, we can calculate the spectral representations of the transverse fields $H_\phi(r_1), H_z(r_1), E_z(r_2^+), H_z(r_2^+)$.

As mentioned above, the spectral expansions of the fields are truncated in order to perform numerical calculations. The truncation is performed by introducing a truncation parameter N and setting

$$\tilde{f}_{i,n}(r) = 0, \quad \text{for} \quad |n| > N. \tag{34}$$

The errors introduced by this truncation are twofold:

1) Higher order harmonics are not contained in the result; and
2) even the obtained coefficients show errors as the coupling with harmonics of order $|n| > N$ has been neglected due to the truncation.

The first kind of error simply represents the well-known effects in truncating Fourier series (e.g., Gibb's phenomenon). The second kind of error, however, is a characteristic error for the presented method. It can be estimated by comparing the results for lower order harmonics for increasing N. We note that the convergence behavior with respect to N significantly depends on the expected behavior of the fields $\tilde{f}_{i,n}$ appearing in the solution vector of (31) for large n. In principle, it would have been possible to establish a system of equations involving, e.g., the spectral coefficients of $E_\phi(r_2^+)$ and $H_\phi(r_2^+)$ rather than $E_z(r_2^+)$ and $H_z(r_2^+)$. However, for the problems considered in this paper, the z-components of the fields were expected to have moderate higher order harmonics in contrast to the ϕ-components. This holds especially for the microstrip case considered below, where, e.g., E_ϕ features a singularity at the strip edge leading to significant higher order harmonics.

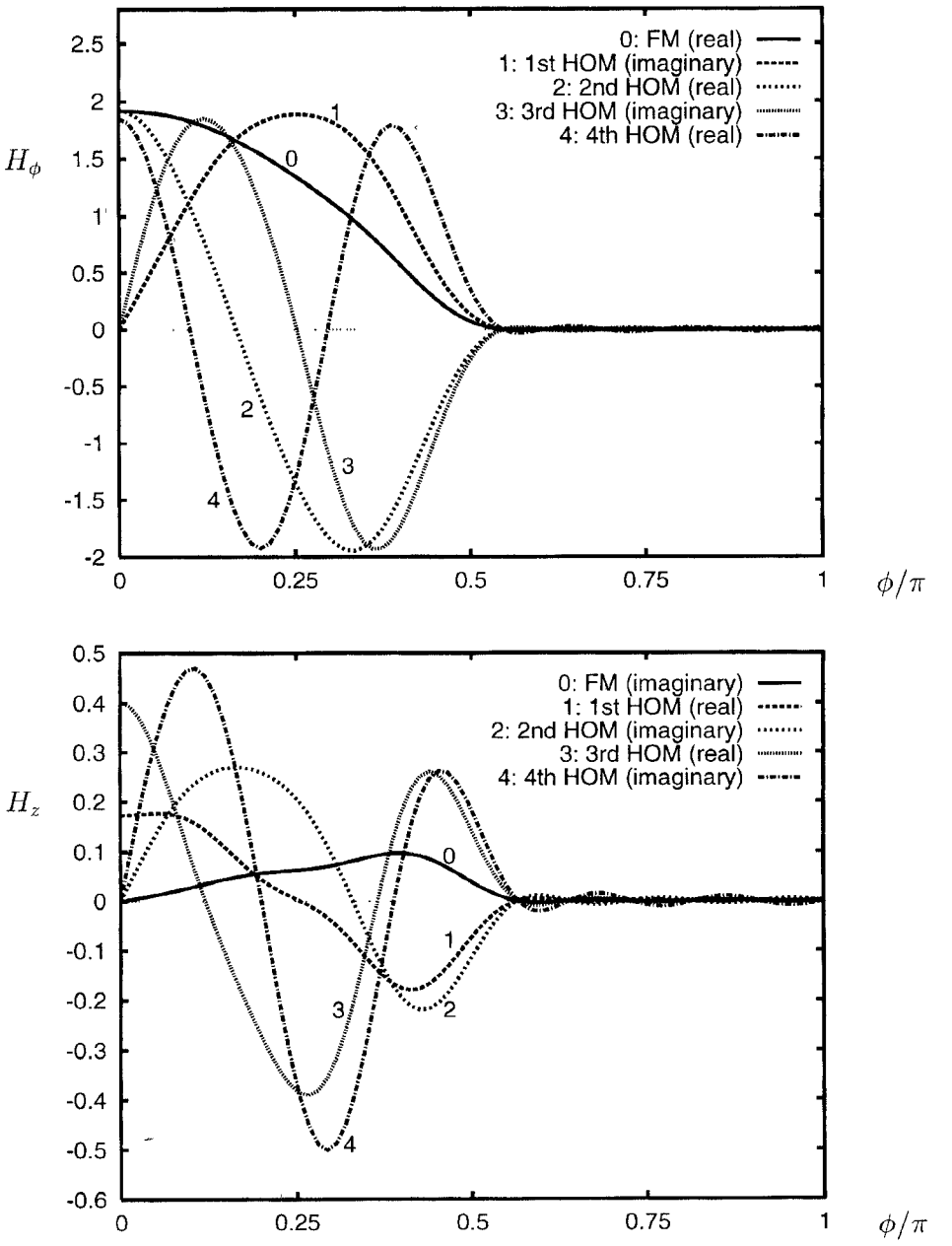

Fig. 4. H_ϕ and H_z at the circumference of the core wire for the fundamental mode (FM) and higher order modes (HOM) of the surface waveguide associated with Fig. 3 ($\omega = 10\omega_{\text{ref}}$).

The influence of the selected unknown fields on the convergence behavior has been reported previously for related planar methods as well [10].

III. Surface Waveguides

As a first application of the method described above, we present the analysis of cylindrical surface waveguides with laterally inhomogeneous layers. Thereby we refer to structures as shown in Fig 1 in the absence of a microstrip metallization. This means, that we are searching for solutions of (31) for vanishing excitation vector (i.e., the right-hand side of (31) is zero). In other words, we are searching for combinations (ω, k_z) yielding a vanishing determinant

$$\det[\underline{\underline{\mathbf{C}}}(\omega, k_z)] = 0 \tag{35}$$

where $\underline{\underline{\mathbf{C}}}$ denotes the system matrix given in (31). For an increasing number of considered harmonics, the dimension of $\underline{\underline{\mathbf{C}}}$ becomes comparably large, leading to well-known numerical problems in the evaluation of determinants. One can overcome these problems by using rescaling algorithms but then one is still confronted with a possible nonsmooth behavior of the determinant as the parameters ω and k_z are varied. Previously we reported a simple alternative method by searching for the poles in the spectral fields for a given excitation [8]. This

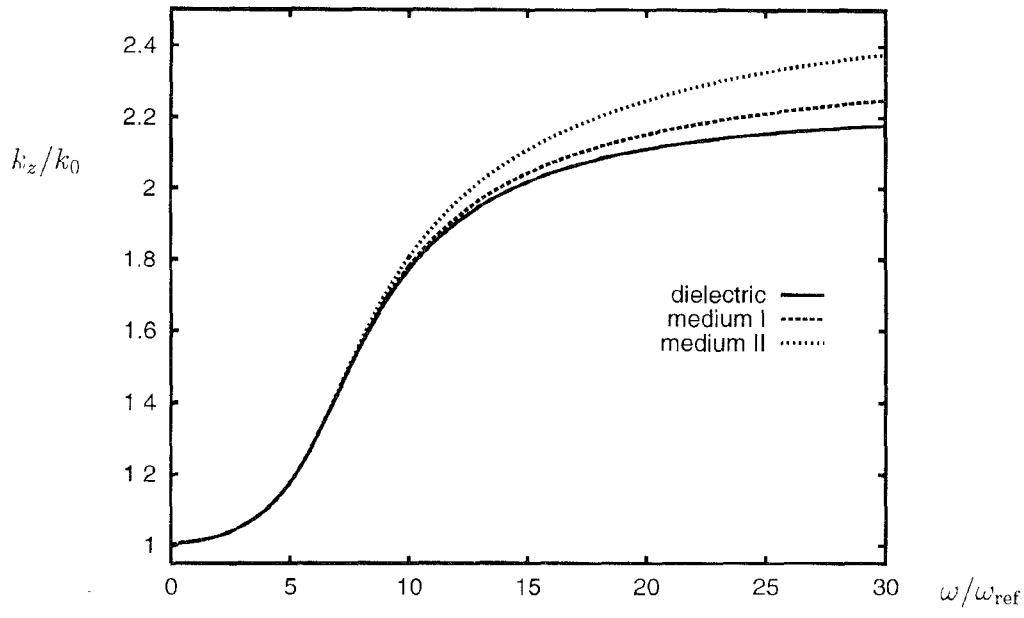

Fig. 5. Fundamental surface wave mode dispersion curves for a partially coated wire for different chiral parameters (see text)

approach includes the risk that some determinant zeros get lost as they are compensated by numerator zeros in the solution for the spectral field coefficients. However, as we are dealing with unknowns and excitation vectors that feature a distinct physical interpretation, we can easily predict what mode will be excited by what excitation.

Typically we chose all elements of one of the four excitation currents to be one, which corresponds to the calculation of the fields due to a delta current source at $\phi = 0$. The corresponding solution for the fields then can be interpreted as a particular set of Green's functions.

In the following examples, we consider a layer of the form shown in Fig. 2 where the substrate only extends over an angle $\Delta\phi$ (here we consider the surface wave case where no strip metallization is present). Note that an additional inhomogeneity with respect to r is included in our approach (see (22)). However, in the following we will restrict ourselves to piecewise constant media with respect to the radial direction. The homogeneous case $\Delta\phi = 2\pi$ represents a "Goubau surface waveguide" which, for the case of isotropic substrate media, has been intensively studied in the past [11]. In this special case the wavenumber can be obtained as the root of a transcendental function which can be written in closed form.

To validate the approach, we first investigated an isotropic waveguide made up of a dielectric material with $\varepsilon_r = 5$ coating half the circumference of the core wire, i.e., $\Delta\phi = \pi$. The radii were chosen as $k_{\mathrm{ref}} r_1 = 1$ and $k_{\mathrm{ref}} r_2 = 1.1$, where $k_{\mathrm{ref}} = \omega_{\mathrm{ref}}\sqrt{\varepsilon_0\mu_0}$ denotes the free space wavenumber at a reference frequency ω_{ref}. The following results have been obtained with $L = 6$ and $N = 10$ for the number of sublayers and the truncation parameter, respectively. As the fields are essentially concentrated within the covered region and show sinusoidal-like behavior with respect to ϕ, it is clear that numerical convergence can be achieved for relatively small N especially in case of lower order modes.

Fig. 3 shows the dispersion curves for the fundamental as well as the first four higher order modes where the latter feature a cut off frequency in contrast to the fundamental mode. For comparison, the dispersion curve of the Goubau mode for a homogeneous layer ($\Delta\phi = 2\pi$) is shown as well. As expected, the fundamental mode dispersion curve approaches that of the Goubau surface wave at higher frequencies as well as at very low frequencies where the wavenumbers approach the free-space wavenumber k_0.

Fig. 4 shows the tangential magnetic field components $H_\phi(r_1)$ and $H_z(r_1)$ at $\omega = 10\omega_{\mathrm{ref}}$ that correspond to the surface currents at r_1, $J_z^S(r_1)$ and $-J_\phi^S(r_1)$, respectively. The even modes, i.e., fundamental, 2nd and 4th higher order modes, show symmetric (asymmetric) behavior for $H_\phi(H_z)$ with respect to $\phi = 0$; therefore we show the range $(0, \pi)$, only. The opposite holds for the odd modes (1st and 3rd higher order modes). The scaling of the amplitudes is arbitrary as they represent eigensolutions, the ratio of corresponding H_ϕ and H_z values is given correctly, though. Note that H_ϕ and H_z are 90 degree out of phase. For the even (odd) modes we chose $H_\phi(H_z)$ to be real which means that the corresponding $H_z(H_\phi)$ is purely imaginary.

In Fig. 5 we compare the fundamental modes for the above dielectric case to chiral cases, where the layer medium features additional chiral parameters according to $\xi = -\zeta = -j0.15\sqrt{\varepsilon_0\mu_0}$ (medium I) or $\xi = -\zeta = -j0.3\sqrt{\varepsilon_0\mu_0}$ (medium II). The corresponding fields $H_\phi(r_1)$ and $H_z(r_1)$ at $\omega = 10\omega_{\mathrm{ref}}$ are shown in Fig. 6. In contrast to the pure dielectric case, the chiral media show additional imaginary (real) parts for $H_\phi(H_z)$ which are asymmetric (symmetric) with respect to $\phi = 0$.

Another typical angular inhomogeneity is represented by a nontruncated cylindrical layer ($\Delta\phi = 2\pi$) which is made of bianisotropic material being homogeneous with respect to rectangular coordinates. One can think of a layer produced by

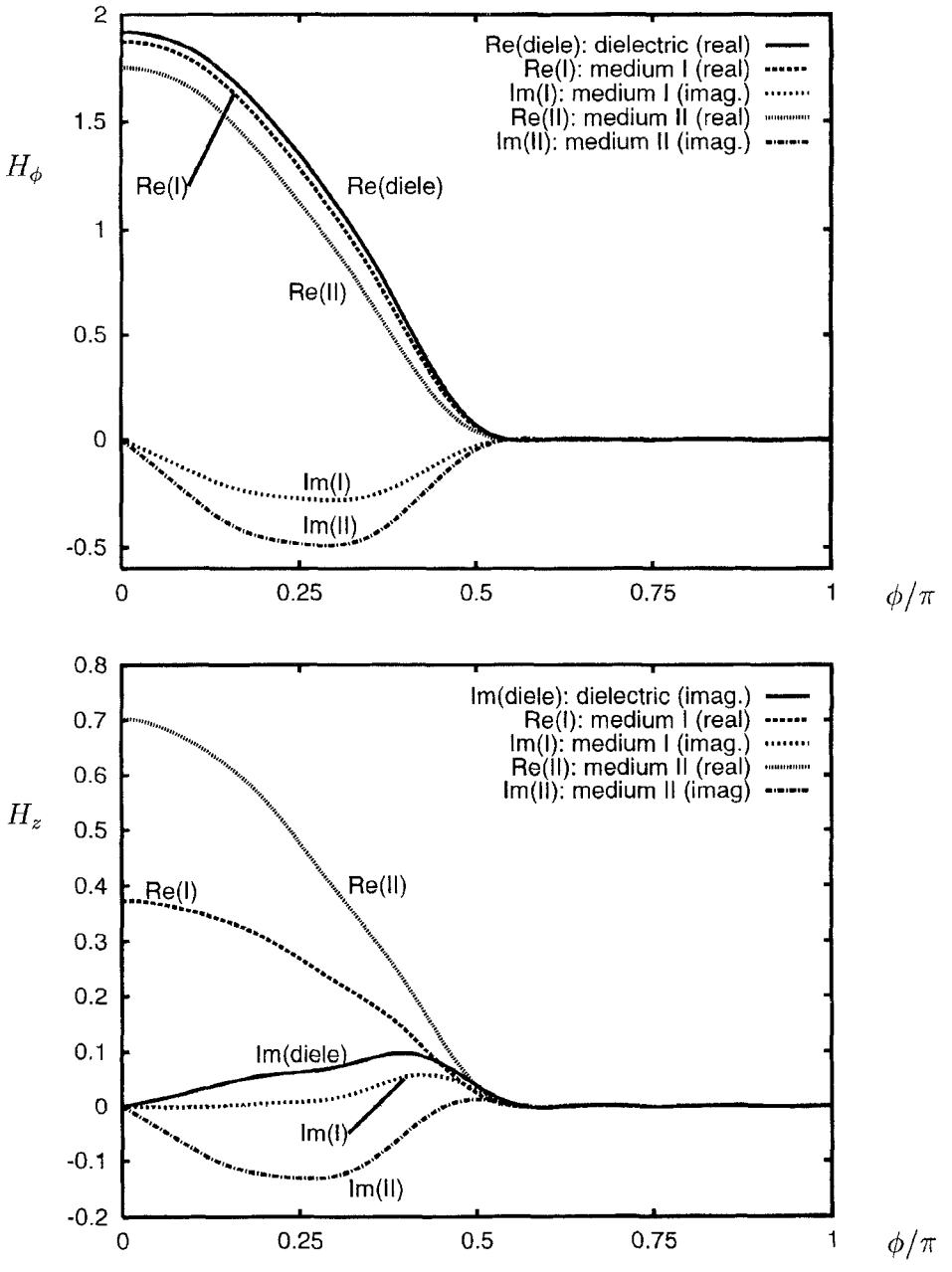

Fig. 6. H_ϕ and H_z at the circumference of the core wire for the fundamental modes in an inhomogeneous surface waveguide: pure dielectric and chiral cases ($\omega = 10\omega_{\mathrm{ref}}$, see also Fig. 5).

cutting a circular cylinder out of a homogeneous, bianisotropic material. Now imagine that a hole is drilled into the center of that cylinder which is then filled with the core wire. In other words, the representation of the tensors $\underline{\underline{\varepsilon}}, \underline{\underline{\mu}}, \underline{\underline{\xi}}$ and $\underline{\underline{\zeta}}$ in the rectangular x, y, z coordinate system is the same at every point within the cylindrical layer. However, their representation in cylindrical coordinates, which actually enters our equations, is given by [2]

$$\underline{\underline{\varepsilon}}_{r,\phi,z} = \underline{\underline{\mathbf{T}}}^T \cdot \underline{\underline{\varepsilon}}_{x,y,z} \cdot \underline{\underline{\mathbf{T}}}, \tag{36}$$

where

$$\underline{\underline{\mathbf{T}}} = \begin{bmatrix} \cos\phi & -\sin\phi & 0 \\ \sin\phi & \cos\phi & 0 \\ 0 & 0 & 1 \end{bmatrix} \tag{37}$$

and analogously for $\underline{\underline{\mu}}$, $\underline{\underline{\xi}}$ and $\underline{\underline{\zeta}}$. Hence the constitutive tensors in cylindrical coordinates are inhomogeneous with respect to ϕ. We considered for example a material obeying

$$\underline{\underline{\mu}}_{x,y,z} = \mu_0 \begin{bmatrix} 4.9 & 0 & 0 \\ 0 & 5 & j0.1 \\ 0 & -j0.1 & 5 \end{bmatrix}, \quad \underline{\underline{\varepsilon}} = \varepsilon_0 \underline{\underline{\mathbf{I}}}, \ \underline{\underline{\xi}} = \underline{\underline{\zeta}} = 0 \tag{38}$$

which is the typical constellation, e.g., for a ferrite with a magnetic bias field in the x-direction. The radii were $k_{\mathrm{ref}} r_1 = 1$ and $k_{\mathrm{ref}} r_2 = 1.1$ and the numerical parameters were chosen as $L = 6$ and $N = 9$.

Fig. 7 shows the dispersion diagrams for the first few modes. All modes, except the fundamental mode, feature

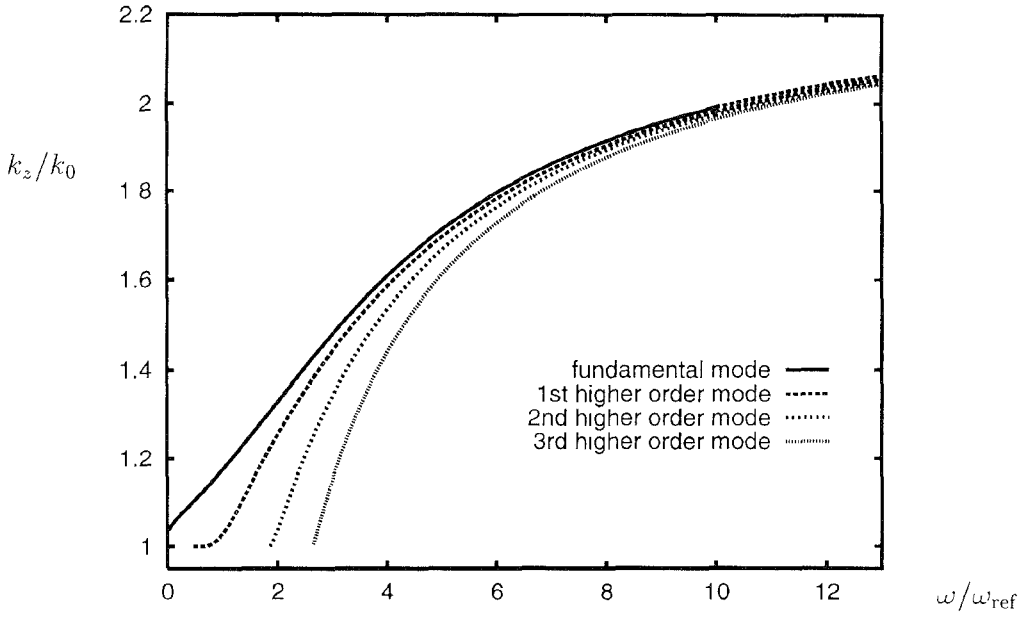

Fig 7. Surface wave dispersion curves for a "ferrite" coated wire.

cut-off frequencies. At low frequencies the field patterns are similar to those one would expect for a homogeneous isotropic coating. Fig. 8 shows the fields $H_\phi(r_1)$ and $H_z(r_1)$ for all modes existing at $\omega = 2\omega_{\mathrm{ref}}$. However, at $\omega = 10\omega_{\mathrm{ref}}$ the patterns look substantially different; Fig. 9 shows the fields $H_\varphi(r_1)$ and $H_z(r_1)$ for the first four modes.

We mention that for a real ferrite, the $\underline{\underline{\mu}}$ tensor is, of course, frequency dependent which can also be handled by the presented method, since the results are computed separately for every frequency point.

IV. Cylindrical Microstrip Lines

Another example for the application of our approach is the analysis of microstrip lines on cylindrical substrates as shown in Fig. 2. We use the method of moments (MoM) to solve for the propagation constants of fundamental and higher order microstrip modes. The surface currents on the strip are expanded in terms of a finite number of basis functions. The expansion coefficients are then determined by enforcing the boundary condition

$$E_\phi = E_z = 0 \tag{39}$$

on the strip in a weighted sense. We used the Galerkin method where the basis functions are also used as testing functions.

The fields generated by the considered basis functions are calculated by solving (31) for multiple right hand sides where each excitation vector accounts for one basis function. The testing of the obtained fields can then be performed conveniently in spectral domain, e.g.

$$A_{lm} = \int_{-\pi}^{\pi} T^{(l)}(\phi) E_z^{(m)}(\phi) d\phi = 2\pi \sum_n \tilde{T}_{-n}^{(l)} \tilde{E}_{z,n}^{(m)} \tag{40}$$

where $E_z^{(m)}(\phi)$ denotes the field E_z due to mth basis function and $T^{(l)}(\phi)$ is the lth testing function. Similarly the fields E_ϕ are tested, where we used the basis functions for $J_z(J_\phi)$ as testing functions for $E_z(E_\phi)$. Enforcing (39) yields the following linear system of equations

$$\sum_{m=1}^{M} A_{lm} c_m = 0 \quad (l = 1 \cdots M) \tag{41}$$

where c_m is the expansion coefficient associated with basis function m. We then solve for the dispersion equation by requiring that the determinant of the system matrix A_{lm} vanishes.

Concerning the choice of basis functions for microstrip problems, a large number of approaches has been presented in the past decades. It turned out, that taking into account the edge condition in the basis functions, may lead to highly accurate results even if only a few basis functions are used. On the other hand, it has been reported that the incorporation of the edge condition is not necessarily required when using a spectral domain MoM [10]. In conventional methods, as they are used for planar microstrip lines, spectral interaction integrals are calculated numerically and hence computational efficiency is increased if less integral evaluations are required (i.e. only a few basis functions are used) and if the Fourier transform of the basis functions is available in closed form. Hence the usage of basis functions considering the edge condition and having closed form Fourier transforms is indicated due to the aforementioned reasons. In our case the situation is somewhat different. The major factor determining computational cost is the truncation limit N. In the spectral domain, basis functions featuring edge singularities show weaker decay for large spectral indices n compared to basis functions without edge singularities. For instance, typical basis functions for J_z with and without edge conditions are (for $|\phi| > w/2$ we have $B_1 = B_2 = 0$, where w denotes the stripwidth angle in

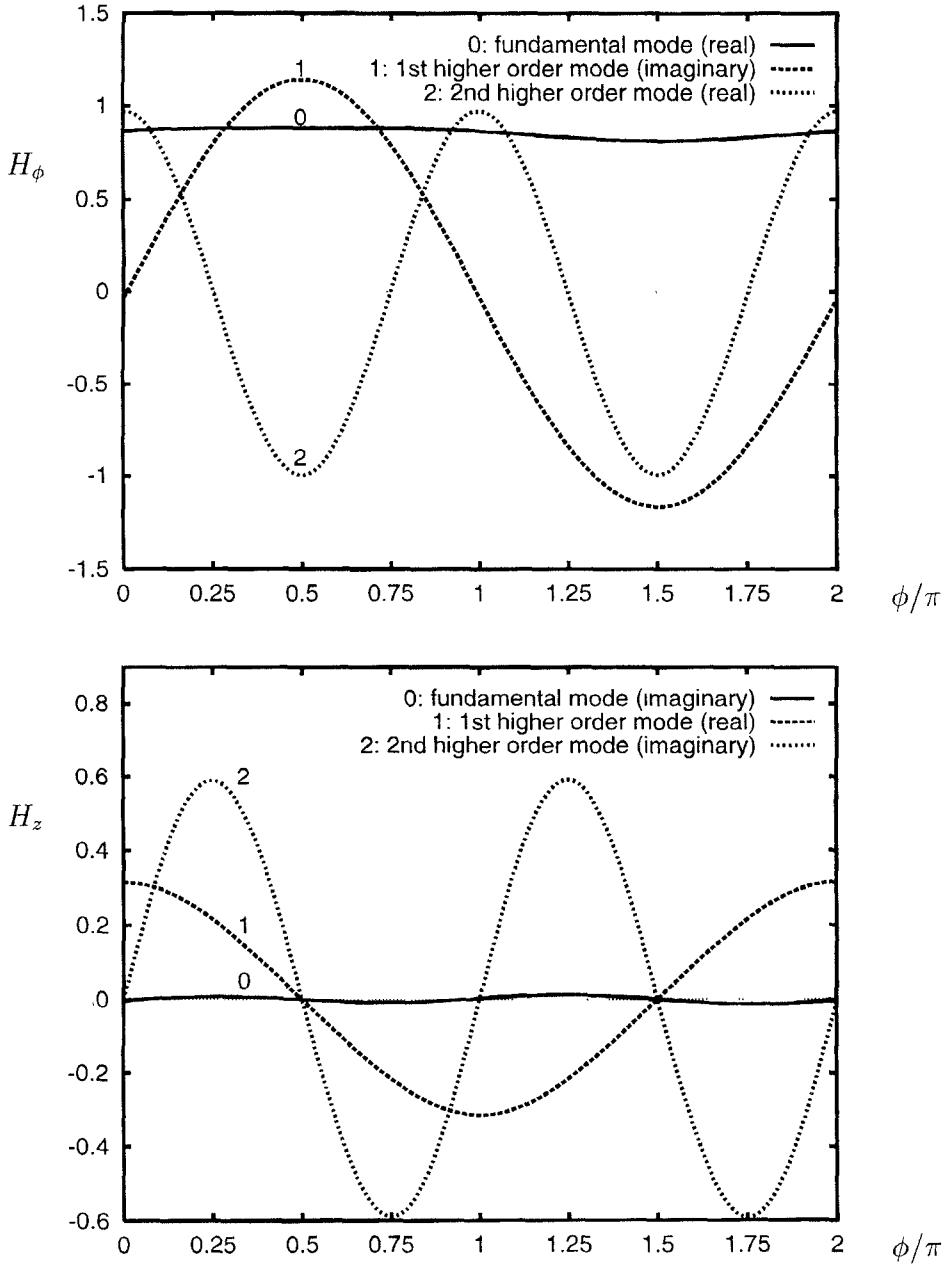

Fig. 8. H_ϕ and H_z at the circumference of the core wire for the first three surface wave modes in a "ferrite" coated wire ($\omega = 2\omega_{\mathrm{ref}}$, see also Fig. 7).

radians, see Fig. 2)

$$B_1(\phi) = \frac{1}{\sqrt{1-\left(\frac{2\phi}{w}\right)^2}} \leftrightarrow \check{B}_{1,n} = \frac{w}{4} J_0\Big(\frac{wn}{2}\Big), \quad (42)$$

$$B_2(\phi) = 1 \leftrightarrow \check{B}_{2,n} = \frac{1}{\pi}\frac{\sin(\frac{wn}{2})}{n} \quad (43)$$

where J_0 denotes the ordinary Bessel function of first kind and zeroth order. The envelope of $\check{B}_{1,n}$, which is the Fourier coefficient of the basis function with incorporated edge condition, behaves like $1/\sqrt{n}$ as $n \to \infty$ while that of $\check{B}_{2,n}$ (no edge condition incorporated) behaves as $1/n$. In order to keep the number of required space harmonics small, basis functions without edge singularities have been used. For the sample results given below, we used a simple "classical" set given in [12] (see Fig. 10).

Let us first consider a bi-isotropic (chiral) medium with $\varepsilon = 5\varepsilon_0, \mu = \mu_0$, $\xi = -j0.3\sqrt{\varepsilon_0\mu_0}$ and $\zeta = j0.3\sqrt{\varepsilon_0\mu_0}$. The geometry is that shown in Fig. 2 with $w = 0.4\pi$, $k_{\mathrm{ref}}r_1 = 1, k_{\mathrm{ref}}r_2 = 1.1$ and $\Delta\phi = \pi$. Fig. 11 shows the convergence behavior for one up to four used basis functions (in the order given in Fig. 10) at $\omega = \omega_{\mathrm{ref}}$ and $\omega = 10\omega_{\mathrm{ref}}$ for the fundamental mode. In the case $\omega = \omega_{\mathrm{ref}}$ numerical convergence is achieved for about $N > 16$ in all cases (with $L = 6$ sublayers) and the accuracy that can be achieved with our simple set of basis functions seems to be in the order of a few percent at this frequency. At higher frequencies the convergence behavior turned out to be significantly improved (see Fig. 11 for $\omega = 10\omega_{\mathrm{ref}}$, note the different scaling of k_z/k_0

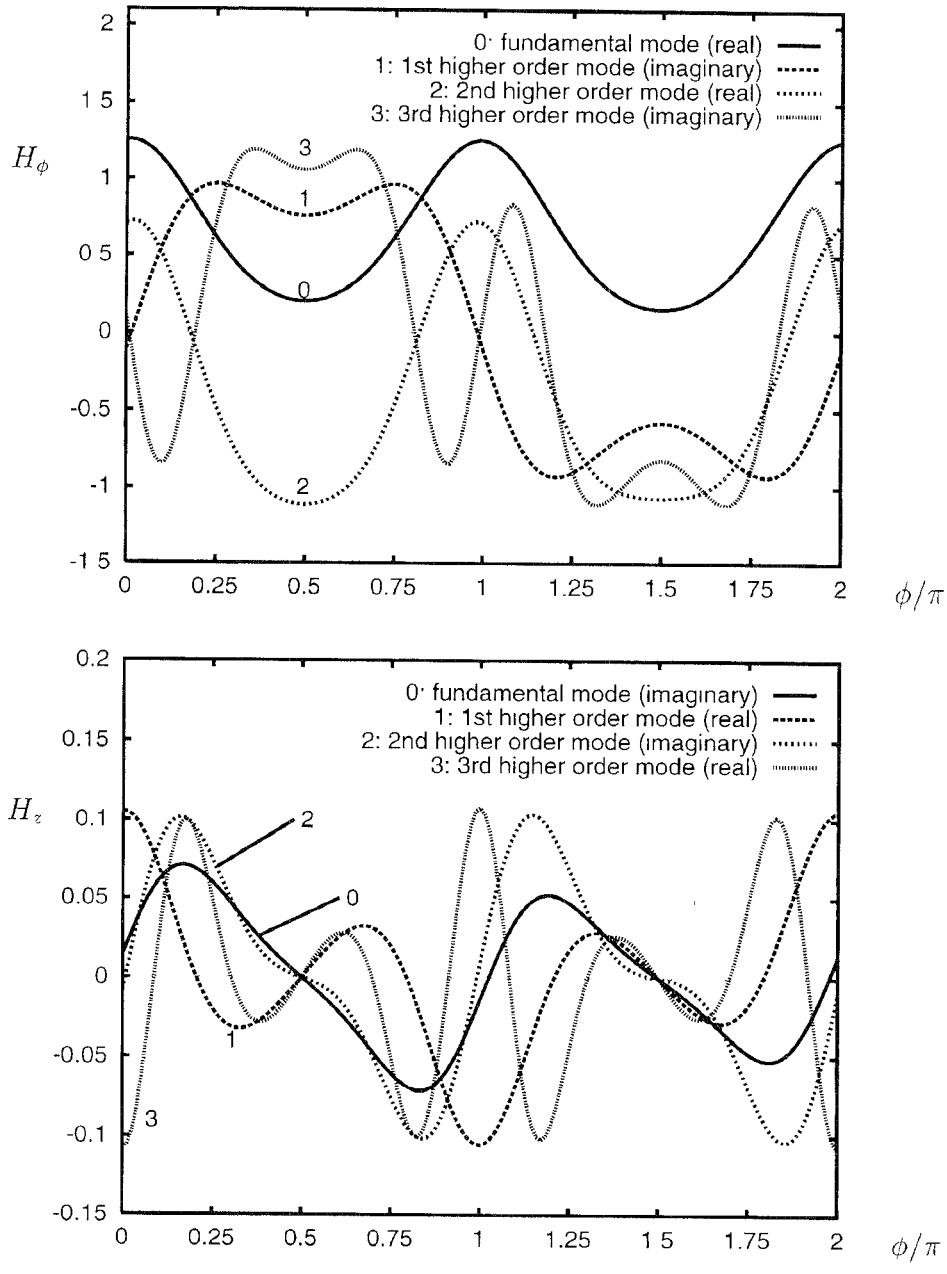

Fig. 9. As Fig. 8 but $\omega = 10\omega_{\mathrm{ref}}$

compared to the case $\omega = \omega_{\mathrm{ref}}$). During the calculation of the dispersion curves it was found, however, that at certain frequencies the convergence limit for the case of four basis functions ($M = 4$) can be considerably higher than for calculations with less than four basis functions. On the other hand, for the fundamental mode even one basis function seems to yield stable and relatively accurate results which confirms the experience from planar microstrip calculations [10].

Fig. 12 shows the dispersion curves of the fundamental mode (calculated with $M = 1$) and a higher order mode ($M = 3$). $N = 28$ was chosen as truncation parameter. Note that the choice of symmetric basis functions for J_z allows the computation of higher order modes with symmetric longitudinal and asymmetric transverse currents, only. For comparison, the related dispersion curves for an ordinary isotropic medium with $\varepsilon = 5\varepsilon_0, \mu = \mu_0, \xi = \zeta = 0$ are shown. We remark that the choice of frequency independent material parameters for our computational example (especially for ξ and ζ) is, of course, not physically realistic but quite common for sample calculations. We also note that the results previously obtained for the homogeneous planar case [13] show that the wavenumbers for different chirality parameters tend to the same value in the zero frequency limit in contrast to the result shown in Fig. 12. This is *not* related to the fact that we here consider circular or inhomogeneous substrates, but simply caused by the alternative set of constitutive equations used in [13].

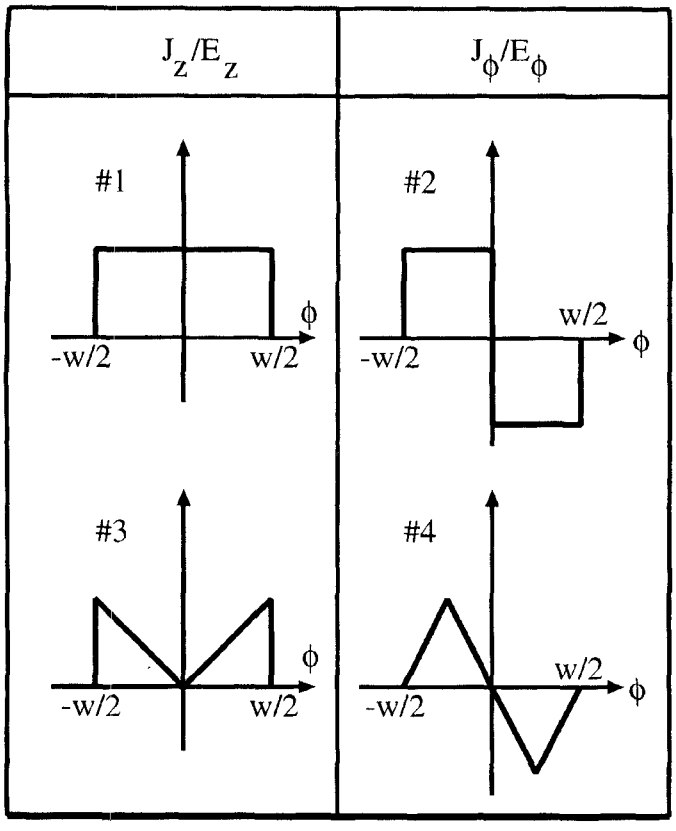

Fig. 10. Basis/testing functions used for the microstrip analysis.

Finally let us consider a uniaxial bianisotropic medium with

$$\underline{\underline{\varepsilon}}_{x,y,z} = \varepsilon_0 \begin{bmatrix} 5 & 0 & 0 \\ 0 & 5 & 0 \\ 0 & 0 & 4 \end{bmatrix}, \quad \underline{\underline{\mu}} = \mu_0 \underline{\underline{\mathbf{I}}},$$
$$\underline{\underline{\xi}}_{x,y,z} = -j\sqrt{\varepsilon_0\mu_0} \begin{bmatrix} 0.3 & 0 & 0 \\ 0 & 0.3 & 0 \\ 0 & 0 & 0.2 \end{bmatrix}, \quad \underline{\underline{\zeta}} = -\underline{\underline{\xi}}. \tag{44}$$

Note that a medium being uniaxial with respect to z features the same representation of the tensors in the cylindrical coordinate frame. The geometry data were $w = 0.4\pi, k_{\text{ref}} r_1 = 1$ and $k_{\text{ref}} r_2 = 1.2$. Fig. 13 shows the dispersion curves for the fundamental and a higher order mode (HOM) for $M = 3, N = 28, L = 10$ and two different choices for $\Delta\phi$, $\Delta\phi = 0.6\pi$ (geometry I) and $\Delta\phi = 0.4\pi$ (geometry II). Note that in the latter case the layer width is equal to the stripwidth such that the strip covers the entire substrate. In Fig. 13 we also show the dispersion curve for the fundamental surface wave mode (SWM). In the homogeneous planar case, HOM's show cutoff as soon as they reach the SWM dispersion curve. This is due to leakage into surface waves for $k_{z,\text{HOM}} < k_{z,\text{SWM}}$, since surface waves traveling away at some angle from the microstrip line are launched [14]. Due to the circular geometry in our case, the only existing SWM's of course travel in the z-direction as well and no leakage into surface waves can occur. Hence bounded HOM's exist even for $k_{z,\text{HOM}} < k_{z,\text{SWM}}$. In the case of geometry I the dispersion curve for the calculated HOM crosses the dispersion curve of the surface wave mode, while for geometry II it lies below the corresponding SWM in the entire frequency range shown. The second limit for leakage is given by $k_{z,\text{HOM}} < k_0$ and corresponds to leakage into space waves. This limit is present in the circular case as well and determines the cut-off for HOM's.

We remark that the method is not restricted to the uniaxial case, only. In the general case, the Fourier coefficients related to functions $g(r, \phi)$ (see (7)), which are composed of the inhomogeneous material parameters, are determined numerically (this has also been done in the "ferrite" surface wave example in the foregoing section).

Finally we mention that the chosen simple set of basis functions served well for demonstrating the applicability of the approach to microstrip problems with moderate computational effort. The extension of the method to more sophisticated sets of basis functions is straightforward. The observed convergence behavior can be qualitatively compared to several results that have been obtained earlier for planar microstrip configurations; a review on such works can be found in [10].

V. Conclusion

A propagator matrix approach for the treatment of problems involving cylindrical, inhomogeneous, and bianisotropic layers has been presented. The method is based upon a spectral technique, leading to infinite-dimensional matrix equations in the spectral domain. By truncating the occuring matrices, an approximation for the propagator matrix for the transverse fields in an inhomogeneous bianisotropic layer can be calculated. We showed the application of the method to cylindrical surface-wave problems as well as to microstrip problems. The pecularities of the approach including the convergence behavior have been discussed. Several sample results show the applicability of the method.

Appendix

The Matrix Operator $\underline{\underline{\mathcal{L}}}$

Formally, Maxwell's equations in cylindrical coordinates can be obtained from those written in rectangular coordinates (primed in the following). Inspection of the curl operator in cylindrical coordinates

$$\nabla \times \mathbf{A} = \begin{bmatrix} 0 & -\frac{\partial}{\partial z} & \frac{1}{r}\frac{\partial}{\partial \phi} \\ \frac{\partial}{\partial z} & 0 & -\frac{\partial}{\partial r} \\ -\frac{1}{r}\frac{\partial}{\partial \phi} & \frac{1}{r}\frac{\partial}{\partial r} r & 0 \end{bmatrix} \cdot \begin{bmatrix} A_r \\ A_\phi \\ A_z \end{bmatrix}. \tag{45}$$

shows similarity with that of a rectangular coordinate system. The picture is essentially disturbed by the term $1/r\,\partial/\partial r\,r$ which prevents the operator matrix from being antisymmetric. The situation can be clarified by considering the operator identity

$$\frac{1}{r}\frac{\partial}{\partial r} r = \frac{1}{r} + \frac{\partial}{\partial r} \tag{46}$$

which allows us to write an antisymmetric operator matrix on the left hand sides of (1) and (2) provided that the disturbing $1/r$ terms are moved to the right hand sides. Doing so, and substituting the derivative operators as

$$\frac{1}{r}\frac{\partial}{\partial \phi} \to \frac{\partial}{\partial x'}, \frac{\partial}{\partial z} \to \frac{\partial}{\partial y'}, \frac{\partial}{\partial r} \to \frac{\partial}{\partial z'} \tag{47}$$

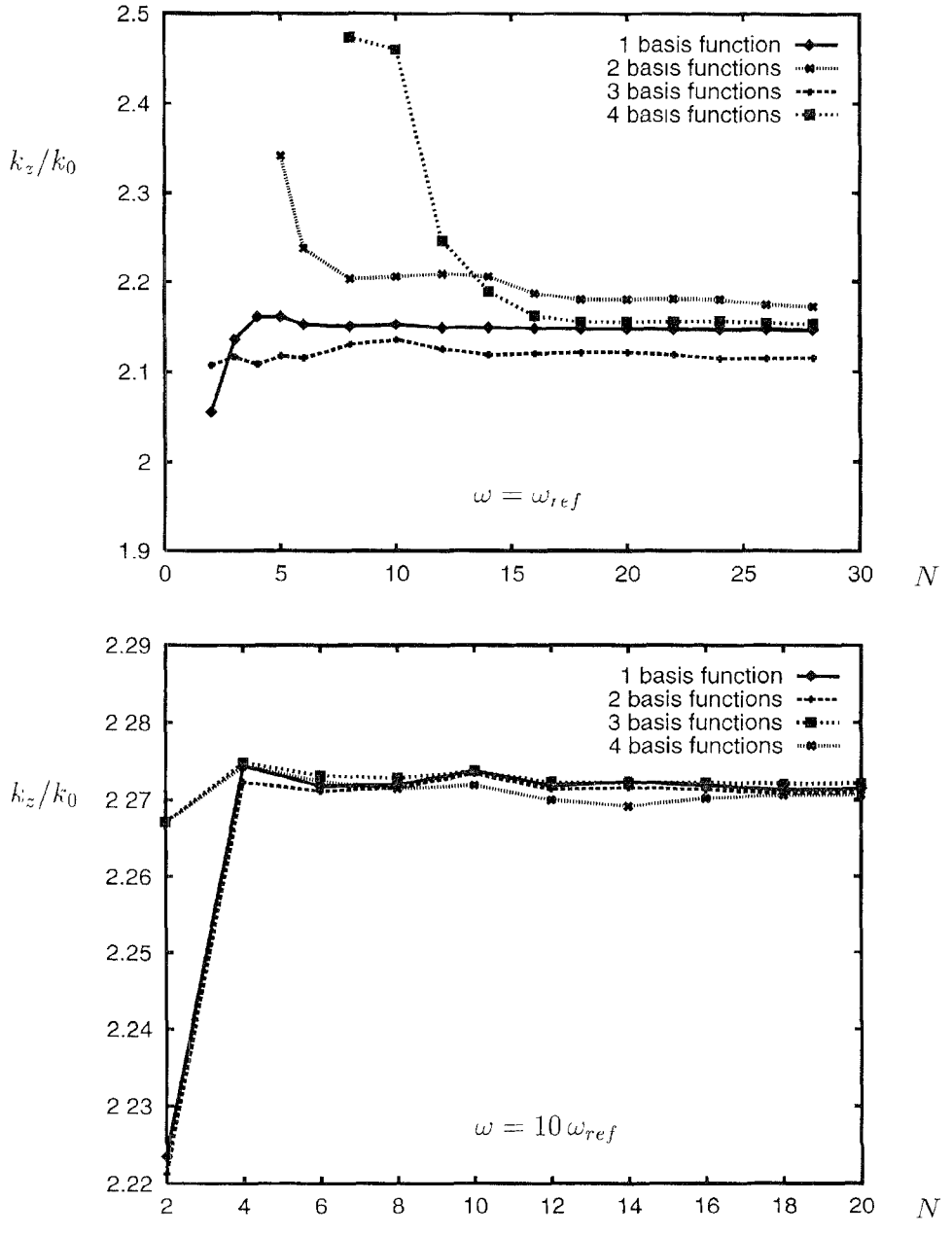

Fig. 11 Convergence behavior with respect to N in the microstrip analysis for different numbers of basis functions at $\omega = \omega_{\mathrm{ref}}$ and $\omega = 10\omega_{\mathrm{ref}}$ (fundamental mode) The number of considered spatial harmonics corresponds to $2N + 1$ Note the different scaling of the k_z/k_0 axes

and the material parameter indices according to

$$\phi \rightarrow x', z \rightarrow y', r \rightarrow z' \tag{48}$$

except for

$$\xi_{z\phi} - \frac{1}{j\omega}\frac{1}{r} \rightarrow \xi_{y'x'}, \quad \zeta_{z\phi} + \frac{1}{j\omega}\frac{1}{r} \rightarrow \zeta_{y'x'} \tag{49}$$

yields Maxwell's equations for a rectangular coordinate system (x', y', z') (in the planar case treated previously [8], [9] the z' axis was assumed to be the axis of stratification; it hence corresponds to r in the current formulation). The additional terms $\pm 1/r$ in (49) are the formal consequence of the procedure described above.

This means, that the operator matrix previously obtained for the rectangular coordinate system [8], [9] can be utilized to construct that in cylindrical coordinates by using the above substitution rules in the other direction. The result reads

$$\mathcal{L}_{11} = -\zeta_{z\phi} - \frac{1}{j\omega r} + (\partial_\phi - \zeta_{zr})A - \mu_{zr}B, \tag{50}$$

$$\mathcal{L}_{21} = \zeta_{\phi\phi} + (\partial_z + \zeta_{\phi r})A + \mu_{\phi r}B. \tag{51}$$

$$\mathcal{L}_{31} = \varepsilon_{z\phi} + \varepsilon_{zr}A + (\partial_\phi + \xi_{zr})B. \tag{52}$$

$$\mathcal{L}_{41} = -\varepsilon_{\phi\phi} - \varepsilon_{\phi r}A + (\partial_z - \xi_{\phi r})B, \tag{53}$$

$$\mathcal{L}_{12} = -\zeta_{zz} + (\partial_\phi - \zeta_{zr})C - \mu_{zr}D, \tag{54}$$

$$\mathcal{L}_{22} = \zeta_{\phi z} + (\partial_z + \zeta_{\phi r})C + \mu_{\phi r}d, \tag{55}$$

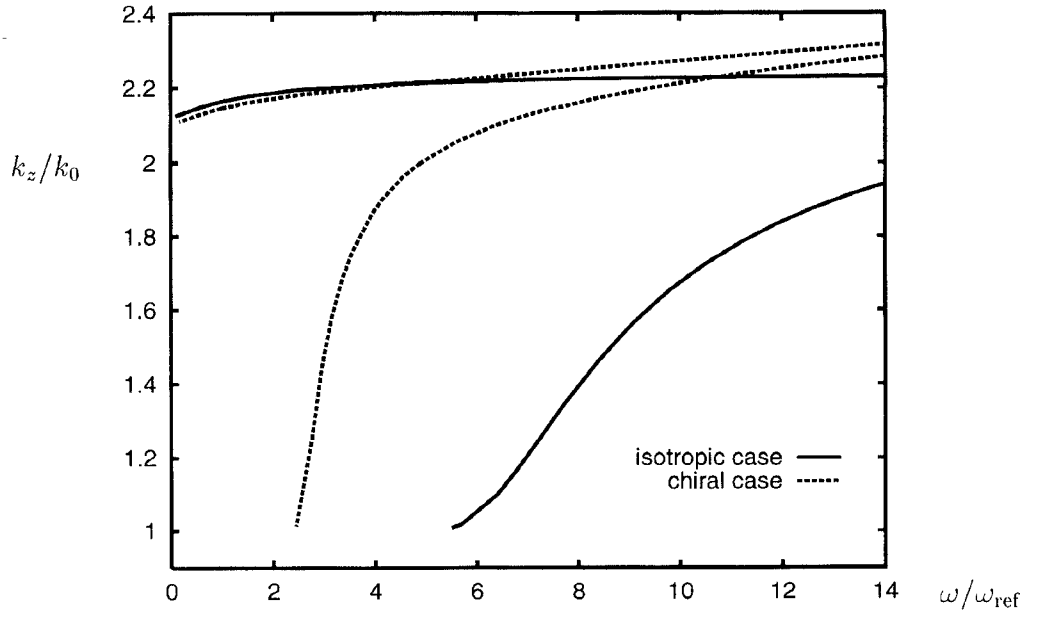

Fig. 12. Microstrip dispersion curves for an inhomogeneously coated wire, isotropic, and chiral case (see text).

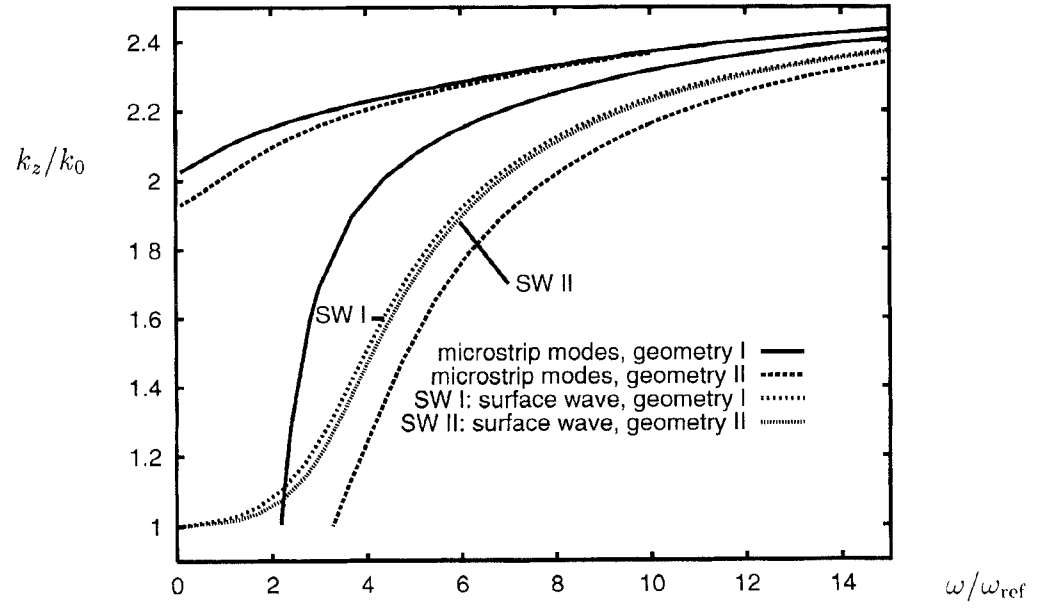

Fig. 13. Microstrip dispersion curves for an inhomogeneously coated wire with bianisotropic substrate for two different substrate widths ($\Delta\phi = 0.6\pi$ and 0.4π for geometry I and II, respectively).

$$\mathcal{L}_{32} = \varepsilon_{zz} + \varepsilon_{zr}C + (\partial_\phi + \xi_{zr})D, \tag{56}$$

$$\mathcal{L}_{42} = -\varepsilon_{\phi z} - \varepsilon_{\phi r}C + (\partial_z - \xi_{\phi r})D, \tag{57}$$

$$\mathcal{L}_{13} = -\mu_{z\phi} + (\partial_\phi - \zeta_{zr})E - \mu_{zr}F, \tag{58}$$

$$\mathcal{L}_{23} = \mu_{\phi\phi} + (\partial_z + \zeta_{\phi r})E + \mu_{\phi r}F, \tag{59}$$

$$\mathcal{L}_{33} = \xi_{z\phi} - \frac{1}{j\omega r} + \varepsilon_{zr}E + (\partial_\phi + \xi_{zr})F, \tag{60}$$

$$\mathcal{L}_{43} = -\xi_{\phi\phi} - \varepsilon_{\phi r}E + (\partial_z - \xi_{\phi r})F, \tag{61}$$

$$\mathcal{L}_{14} = -\mu_{zz} + (\partial_\phi - \zeta_{zr})G - \mu_{zr}H, \tag{62}$$

$$\mathcal{L}_{24} = \mu_{\phi z} + (\partial_z + \zeta_{\phi r})G + \mu_{\phi r}H, \tag{63}$$

$$\mathcal{L}_{34} = \xi_{zz} + \varepsilon_{zr}G + (\partial_\phi + \xi_{zr})H, \tag{64}$$

$$\mathcal{L}_{44} = -\xi_{\phi z} - \varepsilon_{\phi r}G + (\partial_z - \xi_{\phi r})H \tag{65}$$

where

$$A = -\frac{\varepsilon_{r\phi}\mu_{rr}}{d_r} - \frac{\xi_{rr}(\partial_z - \zeta_{r\phi})}{d_r}, \tag{66}$$

$$B = \frac{\varepsilon_{r\phi}\zeta_{rr}}{d_r} + \frac{\varepsilon_{rr}(\partial_z - \zeta_{r\phi})}{d_r}, \tag{67}$$

$$C = -\frac{\varepsilon_{rz}\mu_{rr}}{d_r} - \frac{\xi_{rr}(-\partial_\phi - \zeta_{rz})}{d_r}, \tag{68}$$

$$D = \frac{\varepsilon_{rz}\zeta_{rr}}{d_r} + \frac{\varepsilon_{rr}(-\partial_\phi - \zeta_{rz})}{d_r}, \tag{69}$$

$$E = \frac{\mu_{r\phi}\xi_{rr}}{d_r} + \frac{\mu_{rr}(-\partial_z - \xi_{r\phi})}{d_r}, \tag{70}$$

$$F = -\frac{\varepsilon_{rr}\mu_{r\phi}}{d_r} - \frac{\zeta_{rr}(-\partial_z - \xi_{r\phi})}{d_r}, \tag{71}$$

$$G = \frac{\mu_{rz}\xi_{rr}}{d_r} + \frac{\mu_{rr}(\partial_\phi - \xi_{rz})}{d_r}, \tag{72}$$

$$H = -\frac{\varepsilon_{rr}\mu_{rz}}{d_r} - \frac{\zeta_{rr}(\partial_\phi - \xi_{rz})}{d_r} \tag{73}$$

and

$$d_r = \varepsilon_{rr}\mu_{rr} - \xi_{rr}\zeta_{rr}, \tag{74}$$

$$\partial_\phi = \frac{1}{j\omega r}\frac{\partial}{\partial\phi}, \partial_z = \frac{1}{j\omega}\frac{\partial}{\partial z}. \tag{75}$$

Note that operators occuring in the numerator of fractions do not act on the denominator d_r.

REFERENCES

[1] J. A. Kong, *Electromagnetic Wave Theory*. New York: Wiley, 2nd Ed., 1990.

[2] W. C. Chew, *Waves and Fields in Inhomogeneous Media*. New York: Van Nostrand Reinhold, 1990.

[3] C. M. Krowne, "Fourier transformed matrix method of finding propagation characteristics of complex anisotropic layered media," *IEEE Trans. Microwave Theory Tech.*, vol. MTT-32, pp. 1617–1625, Dec. 1984.

[4] C. H. Chan and R. Mittra, "Analysis of a class of cylindrical multiconductor transmission lines using an iterative approach," *IEEE Trans. Microwave Theory Tech.*, vol. 35, no. 4, pp. 415–424, 1987.

[5] F. Medina and M. Horno, "Spectral and variational analysis of generalized cylindrical and elliptical strip and microstrip lines," *IEEE Trans. Microwave Theory Tech.*, vol. 38, no. 9, pp. 1287–1293, 1990.

[6] H. A. Auda and A. Z. Elsherbeni, "Multiple microstrip lines on a multilayered cylindrical dielectric substrate on a perfectly conducting wedge," *IEEE Trans. Microwave Theory Tech.*, vol. 41, no. 6/7, pp. 1037–1043, 1993.

[7] K.-L. Wong, Y.-T. Cheng, and J.-S. Row, "Analysis of a cylindrical-rectangular microstrip structure with an airgap," *IEEE Trans. Microwave Theory Tech.*, vol. 42, no. 6, pp. 1032–1037, 1994.

[8] B. Jakoby and A. R. Baghai-Wadji, "Analysis of bianisotropic layered structures with laterally periodic inhomogeneities—An eigenoperator formulation," *IEEE Trans. Antennas Propagat.*, submitted, Sept. 1994.

[9] B. Jakoby, "Analysis of electromagnetic fields in stratified complex media," Ph.D. Thesis, Vienna Univ. of Technology, 1994.

[10] D. Mirshekar-Syahkal, *Spectral Domain Methods for Microwave Integrated Circuits*. Chichester, UK: Wiley, 1990.

[11] R. E. Collin, *Field Theory of Guided Waves*, 2nd ed. Piscataway: IEEE Press, 1991.

[12] T. Itoh and R. Mittra, "Spectral domain approach for calculating the dispersion characteristics of microstrip lines," *IEEE Trans. Microwave Theory Tech.*, pp. 496–499, July 1973.

[13] M. S. Kluskens and E. H. Newman, "A microstrip line on a chiral substrate," *IEEE Trans. Microwave Theory Tech.*, vol. 39, pp. 1889–1891, Nov. 1991.

[14] A. A. Oliner and K. S. Lee, "The nature of the leakage from higher order modes on microstrip line," in *IEEE MTT Microwave Symp. Dig.*, 1986, pp. 57–60.

Bernhard Jakoby (S'90-M'94) was born November 17, 1966 in Neuß, Germany. He received the Dipl.-Ing. and the Ph.D. degrees both from the Vienna University of Technology, Austria, in 1991 and 1994, respectively.

From 1989 to 1991 he worked as a Tutor (Teaching Assistant) at the Institute of Communication- and Radio-Frequency Engineering, and from 1991 to 1994 as a Research Assistant at the Institute of Electronics (IAEE) at the same university. Since August 1994, he has been a Guest Scientist at the University of Ghent, Belgium, thanks to an Erwin Schrödinger grant from the Austrian Fund for Scientific Research (FWF). His research interests are numerical and analytical methods as well as complex media in electromagnetics.

Daniël De Zutter (M'92) for a photograph and biography, see this issue, page 207.